ChemComm

COMMUNICATION

Published on 27 August 2026

Cite this: DOI: 10.1039/d6cc04777g

Received 19th July 2026,
Accepted 10th August 2026

DOI: 10.1039/d6cc04777g

rsc.li/chemcomm

Linear dianionic lanthanidocenes: divalent group 14 bis(metallolediide) lanthanide sandwich complexes

Xiaofei Sun, †[a] Maxim Leskov,†[a] Sebastian Gillhuber,[a] Chiara Kirchner,[a] Masaichi Saito,[b] Florian Weigend *[c] and Peter W. Roesky *[ade]

We present a new class of linear dianionic sandwich-type species of Sm(II), Eu(II) and Yb(II), in which the central metal ion is exclusively coordinated by two planar dianionic heterocycles. These complexes were synthesized by salt metathesis. Treatment with (2.2.2)-cryptand or 18-crown-6 afforded ion pairs featuring linear monomeric bis(metalollediide) Ln(II) sandwich dianions.

Sandwich complexes are a fundamental class of compounds in organometallic chemistry. They have found applications in a broad range of fields such as catalysis, medicine, electrochemistry and materials science.[1,2] In general, in sandwich complexes the central metal/metalloid is exclusively bound by two planar, cyclic and π-bonded ligands of various size.[3] Divalent lanthanide sandwich complexes have long been recognized as an important class of compounds. This is not only attributed to their fascinating molecular structures, but also their catalytic activities, photophysical properties, magnetic properties and their potential for small molecule activation.[4–6] Maybe the most prominent species in this series is the Sm derivative $[Sm(C_5Me_5)_2]$ or its THF adducts, which have been widely used as single electron transfer reagents.[6] In general, a typical structural feature of $[Ln(C_5Me_5)_2]$ (Ln = Sm, Eu, Yb) is their bent geometry in the solid state.[6–11] Using bulkier cyclopentadienide (Cp^-) derivatives, linear divalent Ln sandwich complexes such as $[Ln(Cp^{iPr5})_2]$,[12] $[Ln(Cp^{Ph5})_2]$,[13,14] $[Ln(Cp^{iPr5})(C_5Me_5)]$,[15] and $[Ln(Cp^{BIG})_2]$[16] have been obtained. Although commonly described as linear, some of these complexes exhibit static disorder of the Ln(II) ion parallel to the ligands,[14,16] resulting in slight deviations from linearity. Somehow, related to Cp^- complexes are bis cyclononatetraenyl compounds of the divalent lanthanides pioneered by Nakajima and Nocton,[17,18] in which the huge nine-membered ring forces the complexes into a linear geometry.[19]

Cyclooctatetraendiide (Cot^{2-}) derivatives are the second most frequently used ligands in organo-f-element chemistry after Cp^- derivates.[20–22] Depending on the steric demand, classical double-decker, triple- and tetradecker structural motifs,[23–27] or larger cyclic assemblies (cyclocenes) were obtained.[27] Despite the early isolation of homoleptic $[Eu^{II}\{(thf)_3K(C_8H_8)\}_2]$ in 1995,[28] the $[Ln^{II}(C_8H_8)_2]^{2-}$ motif remains rare.[26,28–30]

Recently, group 14 metallole dianions have received tremendous interest as the heavier congeners of cyclopentadienide monoanions.[31–36] Due to their dianionic charge, they form a novel class of highly electron-rich ligands, which are more potent donor ligands compared to monoanionic Cp^- ligands. They have been recently incorporated into the coordination sphere of trivalent lanthanides.[32,37–44] including the first homoleptic trivalent stannolediide sandwich compounds $[Ln(\eta^5\text{-}L^{Sn})_2\text{-}K(thf)_4]$ (Ln = Tb(III), Dy(III); (L^{Sn} = [1,4-bis-(*tert*-butyl-dimethylsilyl)-2,3-bis-phenyl-stannolediide]).[44] K^+ abstraction from these compounds with 18-crown-6 resulted in a Tb(III) complex or a divalent Dy(II) stannolediide complex $[Dy(II)(\eta^5\text{-}L^{Sn})_2][K(18\text{-crown-}6)(thf)_2]_2$. Here the stannolediide acts as a reducing agent and the 1,1′-bistannole-dianion $[(L^{Sn})_2]^{2-}$ was found as byproduct. By this result we felt challenged to explore the coordination group 14 metallolediide to classical divalent lanthanides in a rational approach.

In this work, we introduced two group 14 metallole dianions into the coordination sphere of Ln(II) ions through salt metathesis for the first time. The coordinated potassium cations could be removed and the remaining naked linear dianionic lanthanide sandwich complexes remain stable in the solid state.

[a] *Institute for Inorganic Chemistry, Karlsruhe Institute of Technology, Kaiserstr. 12, 76131, Karlsruhe, Germany. E-mail: roesky@kit.edu*
[b] *Department of Chemistry, Graduate School of Science and Engineering, Saitama University, Shimo-okubo, Sakura-ku, Saitama-city, Saitama, 338-8570, Japan*
[c] *Institute for Quantum Materials and Technologies (IQMT), Karlsruhe Institute of Technology, Kaiserstr. 12, 76131 Karlsruhe, Germany. E-mail: florian.weigend@kit.edu*
[d] *Institute of Nanotechnology, Karlsruhe Institute of Technology, Kaiserstr. 12, 76131 Karlsruhe, Germany*
[e] *Center for Integrated Quantum Science and Technology (IQST), Karlsruhe Institute of Technology, Kaiserstr. 12, 76131 Karlsruhe, Germany*
† These authors contributed equally to this work and share first authorship.

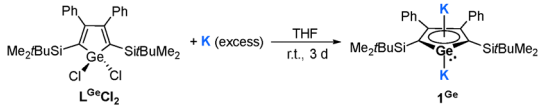

Scheme 1 Synthesis of the dipotassium germole $\mathbf{1^{Ge}}$.

The dipotassium salt of the germole $\mathbf{1^{Ge}}$ was prepared straightforwardly by reduction of the 1,1-chloro-3,4-diphenyl-2,5-bis-(*tert*-butyl-dimethylsilyl)-germole ($\mathbf{L^{Ge}Cl_2}$) with an excess amount of elemental potassium (Scheme 1). Upon reduction, the color of the solution changed from yellow to dark brown. After filtration and evaporation of all volatiles, $[K_2(thf)(\eta^5\text{-}L^{Ge})]$ ($\mathbf{L^{Ge}}$ = [1,4-bis-(*tert*-butyl-dimethylsilyl)-2,3-bis-phenyl-germolediide]) ($\mathbf{1^{Ge}}$) was obtained in 90% yield and was used for the following reactions without further purification. The dipotassio germolediide $\mathbf{1^{Ge}}$ was characterized by multinuclear NMR spectroscopy and single crystal XRD analysis (Fig. 1). Single crystals of $\mathbf{1^{Ge}}$ were obtained from THF/*n*-hexane mixture and the solid-state structure consists of a one-dimensional coordination polymer where each germole ring is η^5-coordinated by two K cations (Fig. 1b). Additionally, one of the two K cations is η^1-coordinated to the Ge lone pair of the neighboring germole ring, thus forming an infinite polymeric chain. The ring planarity (sum of inner angles 540.0°) and the similar C–C bond lengths within the GeC_4 ring hints at the aromatic nature of the germole dianion, and these bonding metrics are comparable to those of smaller derivatives,[45] and the polymeric structure is comparable to that of its heavier stannole analog $[K_2(thf)(\eta^5\text{-}L^{Sn})]$ ($\mathbf{1^{Sn}}$).[44] The ^{1}H NMR spectrum of $\mathbf{1^{Ge}}$ shows a nearly identical spectral profile compared to the $\mathbf{1^{Sn}}$. The singlet in the $^{29}Si\{^1H\}$ NMR spectrum (−3.6 ppm) of $\mathbf{1^{Ge}}$ shows a slight downfield shift compared to stannole congener $\mathbf{1^{Sn}}$ (−5.9 ppm).[44]

The divalent lanthanide diiodides $[Ln^{II}I_2(thf)_2]$ (Ln = Sm, Eu, Yb) were chosen as precursors to react with the dipotassium metallolediides $\mathbf{1^{Ge}}$ and $\mathbf{1^{Sn}}$. The reaction of $\mathbf{1^{Sn}}$ and $[Ln^{II}I_2(thf)_2]$ (Ln = Sm, Eu, Yb) in 2 : 1 molar ratio led to the formation of dark brown solutions along with the formation of insoluble KI (Scheme 2). After workup and crystallization, dark red (Yb) or green crystals (Sm and Eu) were obtained in isolated yields of 41–47%. The solid-state structures of all three isostructural compounds $[Ln^{II}\{(\eta^5\text{-}L^{Sn})K(thf)_3\}_2]$ (Ln = Sm (**2a**), Eu (**2b**), Yb (**2c**)) were elucidated by XRD and the Eu complex **2b**, which is discussed here in detail, is depicted in Fig. 2a (for **2a** and **2c** see SI, Fig. S32 and S34). The molecular structure of **2b** features a neutral homoleptic sandwich complex, in which the Eu atom is located on a center of inversion and perfectly linearly sandwiched between the two stannole rings in η^5-fashion (Ct_{Sn}–Eu–Ct_{Sn} = 180°, Ct = ring centroid). The central structural motif consists of the formally dianionic Eu bis(stannolediide) sandwich structure, in which the two stannole rings are oriented to each other in anti-parallel fashion and the Eu–Ct_{Sn} distance is 2.5428 Å. This is longer when compared with the Eu–Ct distance in $[Eu(Cp^{Ph5})_2]$ (2.489 Å).[14] The two K cations are coordinated by three THF molecules each and additionally to one stannole ring *via* a Sn–K bond. Additionally, the K cations are stabilized by secondary π interactions of the flanking phenyl substituents. In contrast to the stannole system, the germole precursor exhibits limited reactivity towards the divalent lanthanide compounds. No conversion was observed upon reacting $[Yb^{II}I_2(thf)_2]$ with $\mathbf{1^{Ge}}$ in 1 : 2 molar ratio, as verified by NMR spectroscopy. However, under equimolar conditions, complete conversion to the desired complex $[Yb^{II}\{(\eta^5\text{-}L^{Ge})K(thf)_3\}_2]$ (**3**) was achieved. In contrast, no isolable products were obtained for Sm or Eu under either condition. The solid-state structure of the germole based compound **3**

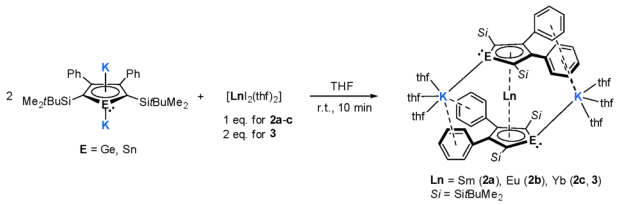

Scheme 2 Synthesis of the neutral Ln bis(stannolediide) complexes **2a–2c** and bis(germolediide) complex **3**.

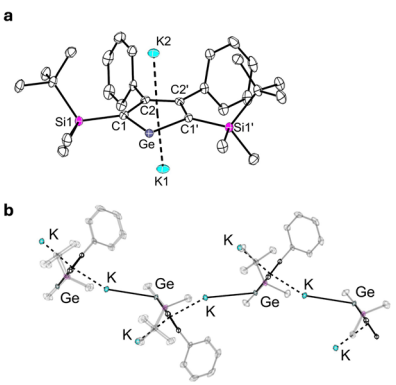

Fig. 1 (a) Asymmetric unit of the coordination polymer of complex $\mathbf{1^{Ge}}$; (b) section of the polymeric chain of complex $\mathbf{1^{Ge}}$. Shown with 50% probability thermal ellipsoids. All hydrogen atoms are omitted for clarity.

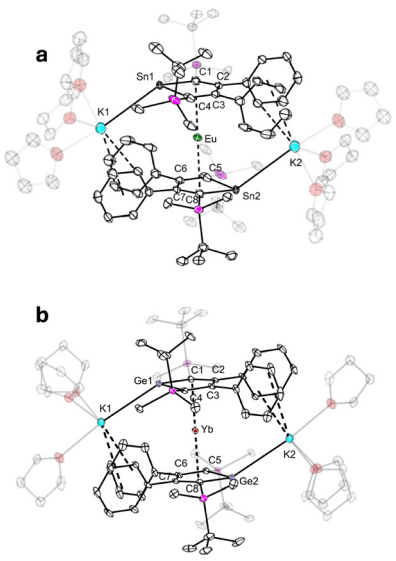

Fig. 2 (a) Molecular structure of the Eu complex **2b** in the solid state shown with 40% probability thermal ellipsoids; hydrogen atoms are omitted for clarity. (b) Molecular structure of the Yb complex **3** in the solid state shown with 50% probability thermal ellipsoids; hydrogen atoms are omitted for clarity.

shows an analogous structural motif to the complexes **2a–c** (Fig. 2 and Fig. S32 and S34). Similarly, the Yb atom is located on an inversion center, perfectly linearly embedded between two germolediide heterocycles in an η^5-binding mode (Ct_{Ge}–Yb–Ct_{Ge} = 180°). The bonding distances within the heterocyclic frameworks, as well as the Yb–Ct distances in **3**, decrease significantly compared to **2c**, a trend that can be rationalized by the smaller ionic radii of the germanium atoms. Noteworthy, compound **3** represents the first structurally characterized monomeric lanthanide-based germole sandwich complex. The NMR spectra (^{1}H, ^{13}C) of the diamagnetic Yb species **2c** and **3** were recorded in THF-d_8. In each instance, several sets of signals were obtained indicating the presence of multiple species in solution (see SI, Fig. S6–S9). However, upon addition of two equivalents of (2.2.2)-cryptand, a clean conversion of the mixture to a single reaction product was detected (see SI, Fig. S11). This sparked our interest in the question whether this reaction product is the homoleptic Ln bis(stannolediide) dianion. In preparative scale, encapsulation of the two potassium cations was achieved by addition of two equivalents of (2.2.2)-cryptand or 18-crown-6 in THF (Scheme 3). This afforded a series of ion pairs [K(2.2.2-crypt)]$_2$[Ln^{II}(η^5-L^{Sn})$_2$] (Ln = Sm (**4a**), Eu (**4b**), Yb (**4c**)) and [K(18-crown-6)]$_2$[Yb^{II}(η^5-L^{Ge})$_2$] (**5**). Using (2.2.2)-cryptand with **3** only resulted in decomposition.

The products were isolated as dark red to purple crystals and XRD analysis revealed that all complexes crystallize as charge-separated ion pairs in the solid state. The dianionic sandwich structures of all four complexes are depicted in Fig. 3. All the Ln metal ions in **4a–4c** are located on a crystallographic inversion center, which results in Ct_{Sn}–Ln–Ct_{Sn} angles of 180°. In contrast, complex **5** crystallizes as an entire molecule in the asymmetric unit, with no inversion center leading to a slight deviation from a perfectly linear arrangement (Ct_{Ge}–Yb–Ct_{Ge} = 178.2°). If the silyl and phenyl groups are neglected, the dianionic sandwich motifs are in first proximity C_{2h} symmetric. The distance between the stannole ligand and the central Ln^{2+} ion decreases from Sm^{2+} to Eu^{2+} to Yb^{2+} (Sm–Ct_{Sn} 2.554, Eu–Ct_{Sn} 2.543, Yb–Ct_{Sn} 2.444 Å), nicely correlating with the decreasing ionic radii along the lanthanide series. Upon complexation, the Yb–Ct_E (E = Ge, Sn) bond distances exhibit a slight elongation due to the decoordination of the bridging potassium atoms. For instance, the Yb–Ct_{Ge} distance increases from 2.382 Å in compound **3** to 2.415 Å in compound **5**. Notably, the ^{1}H NMR spectrum of **5** highlights its low stability, indicating rapid decomposition of the compound and simultaneous formation of the bis(germole) [K(18-crown-6)]$_2$-[(L^{Ge})$_2$] (**6**) (see SI, Fig. S18 and S19).

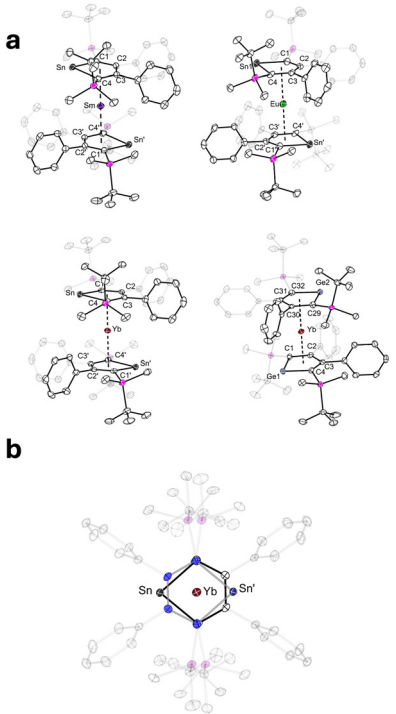

Fig. 3 (a) Molecular structures of the four complexes **4a–4c** and **5** in the solid state shown with 40% probability thermal ellipsoids; (b) top view of the Yb complex **4c**. The cationic part and the hydrogen atoms are omitted for clarity. The two stannole rings are depicted in different colors for clarity.

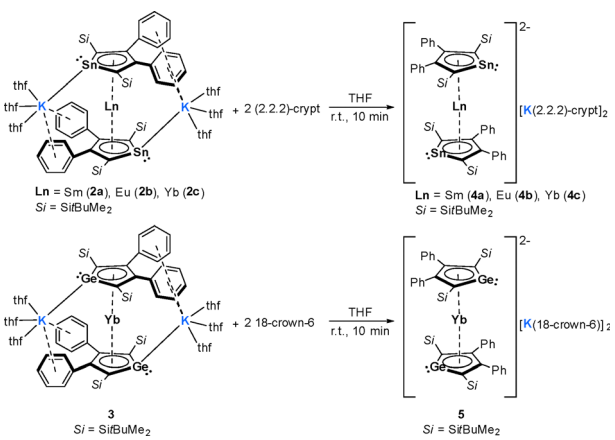

Scheme 3 Synthesis of the dianionic Ln bis(stannolediide) complexes **4a–4c** and dianionic Yb bis(germolediide) complex **5**.

To gain more detailed understanding of the electronic properties of the sandwich complexes, quantum chemical calculation at density functional theory (DFT) level were performed with TURBOMOLE.[46,47] The PBE0 hybrid[48,49] functional in combination with def2-TZVP basis sets[50] were employed. Detailed computational settings and optimized geometries of all compounds are given in the SI (Chapter V). Considerations of the natural population analysis (NPA)[51] charges of the central Ln ions in the complexes **2a–2c** and **4a–c** confirm their expected divalent nature. Values of +1.2 (Sm), +1.2 (Eu) and +1.1 (Yb) elementary charges were found for compounds **2a–2c** and **4a–c**, respectively, which compare well to NPA charges of the metal centers of divalent lanthanide halides of the type Ln^{II}X$_2$ (Ln = Sm, Eu, Yb; X = Cl, Br, I;[27] SI Tables S2 and S3). We note in passing that removing K ions from the direct coordination sphere of the stannole ligands does not influence the charge of the central Ln ions (see SI Table S2). Detailed investigations of the canonical molecular orbitals of the free stannolediide ligand [L^{Sn}]$^{2-}$ and the hypothetical free anion [Yb^{II}(η^5-L^{Sn})$_2$]$^{2-}$ reveal the presence of weak covalent interactions between the

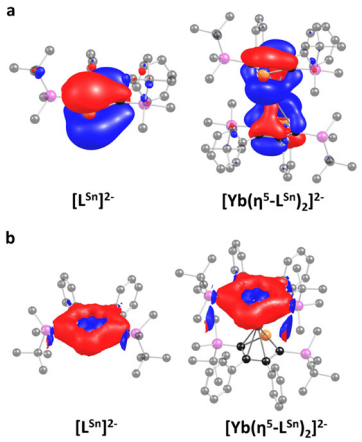

Fig. 4 (a) Highest occupied molecular orbital (HOMO) of the free stannolediide ligand $[L^{Sn}]^{2-}$ (left) and molecular orbital relevant for lanthanide stannole bonding in the hypothetical free anion $[Yb^{II}(\eta^5\text{-}L^{Sn})_2]^{2-}$ (right). (b) Signed modulus of the magnetically induced current density in $[L^{Sn}]^{2-}$ (left) and one stannole ring of $[Yb^{II}(\eta^5\text{-}L^{Sn})_2]^{2-}$ (right). Diatropic contributions are shown in red, paratropic contributions in blue. All contours are drawn at 0.03 atomic units. Details are given in the SI (Chapter V). Hydrogen atoms are omitted and ring substituents are depicted transparently for clarity.

π-system of the stannole ligands and the central Yb ion (see Fig. 4a). Specifically, the highest occupied molecular orbital (HOMO) of the free stannolediide interacts with a vacant orbital of the central Yb ion. Mulliken population analyses (see SI Tables S4 and S5) show that the latter is mainly of d-character, while the HOMO of the free stannole dianion is dominated by contributions of a Sn p-orbital.

Analogous conclusions hold for the compounds **2a–2c** (see SI Fig. S41–S43 and Tables S6–S8) and **4a–4c** (see SI Fig. S44–S46 and Tables S9–S11). The situation resembles observations previously reported for trivalent lanthanide plumbole,[40] stibole and bismole sandwich complexes.[52]

As pointed out above, the ring planarity is retained upon coordination of the stannole ligands and the C–C bond lengths within the SnC_4 ring remain similar, hinting at the aromatic nature of the stannole dianion being retained in the complexes. This is confirmed by calculations of the magnetically induced current density, which probe the aromaticity based on the magnetic criterion, using the GIMIC program.[53–55] The signed modulus of the current density of the free stannolediide and the complex $[Yb^{II}(\eta^5\text{-}L^{Sn})_2]^{2-}$ is shown in Fig. 4b (depictions for Sm and Eu are given in the SI, Fig. S51 and S53). In line with the expected aromatic character, a dominating diatropic current is observed outside the stannole ring, whereas a weaker paratropic ring current flows inside the ring. This holds for the free stannolediide as well as the complex, thus validating that aromaticity is retained upon coordination. The situation is again reminiscent of that in the plumbole,[40] stibole and bismole[52] complexes mentioned above. The qualitative picture resulting from the consideration of the signed modulus of the current density is additionally underpinned by explicit integration of the induced current density to obtain absolute ring current strengths (see SI Chapter V for details). A magnetically induced net diatropic ring current strength of 10 nA T^{-1} is obtained for the free stannolediide which remains basically uninfluenced by coordination to the Ln ions in the complexes (see SI Table S13).

We report the synthesis of homoleptic bis(metallolediide) divalent lanthanide sandwich complexes. Both the neutral sandwich structures in which the potassium cations are coordinated to the sandwich motifs and complexes of the type $[Ln^{II}(\eta^5\text{-}L^{E})_2]^{2-}$ (E = Ge, Sn) have been isolated. Notably, the germanium-based compounds constitute the first structurally characterized monomeric lanthanide germole complexes.

Author contributions

All authors have given approval to the final version of the manuscript. XS and ML synthesized and analyzed all compounds with support from CK. XS and ML conducted X-ray experiments. SG and FW performed the quantum chemical analysis of the bonding situation. MS advised on experiments and theory. PWR originated the idea, supervised the work, and interpreted the results. All authors contributed to the preparation of the manuscript.

Conflicts of interest

There are no conflicts to declare.

Data availability

NMR, IR, and EA data for this paper are available at radar4chem [https://radar.products.fiz-karlsruhe.de] at https://doi.org/10.22000/vzv3gpb7r8261p6ba. Synthesis and characterization, NMR- and IR-spectra, data of X-ray crystallography studies and quantum chemical calculations for this paper are available in the supplementary information (SI). See DOI: https://doi.org/10.1039/d6cc04777g.

CCDC 2570264–2570274 contain the supplementary crystallographic data for this paper.[56a–k]

Acknowledgements

Deutsche Forschungsgemeinschaft (DFG) is acknowledged for financial support within the Reinhart Koselleck-Projekt 440644676, RO 2008/19-1 and the Center for Integrated Quantum Science and Technology (IQST).

References

1 A. Togni and R. L. Halterman, *Metallocenes: Synthesis, Reactivity, Applications*, Wiley-VCH, 1998.
2 M. Patra and G. Gasser, *Nat. Rev. Chem.*, 2017, **1**, 0066.
3 C. A. P. Goodwin, *Inorg. Chem.*, 2024, **63**, 9363–9365.
4 N. Mahieu, J. Piątkowski, T. Simler and G. Nocton, *Chem. Sci.*, 2023, **14**, 443–457.
5 E. Stapf and A. Hinz, *Eur. J. Inorg. Chem.*, 2025, e202400593.
6 S. Schäfer, S. Kaufmann, E. S. Rösch and P. W. Roesky, *Chem. Soc. Rev.*, 2023, **52**, 4006–4045.
7 M. Schultz, C. J. Burns, D. J. Schwartz and R. A. Andersen, *Organometallics*, 2000, **19**, 781–789.

8 W. J. Evans, L. A. Hughes and T. P. Hanusa, *Organometallics*, 1986, **5**, 1285–1291.
9 W. J. Evans, L. A. Hughes and T. P. Hanusa, *J. Am. Chem. Soc.*, 1984, **106**, 4270–4272.
10 P. L. Watson, *J. Chem. Soc., Chem. Commun.*, 1980, 652–653, DOI: 10.1039/C39800000652.
11 T. D. Tilley, R. A. Andersen, B. Spencer, H. Ruben, A. Zalkin and D. H. Templeton, *Inorg. Chem.*, 1980, **19**, 2999–3003.
12 C. A. Gould, K. R. McClain, J. M. Yu, T. J. Groshens, F. Furche, B. G. Harvey and J. R. Long, *J. Am. Chem. Soc.*, 2019, **141**, 12967–12973.
13 A. C. G. Shephard, D. P. Daniels, G. B. Deacon, Z. Guo, F. Jaroschik and P. C. Junk, *Chem. Commun.*, 2022, **58**, 4344–4347.
14 R. P. Kelly, T. D. M. Bell, R. P. Cox, D. P. Daniels, G. B. Deacon, F. Jaroschik, P. C. Junk, X. F. Le Goff, G. Lemercier, A. Martinez, J. Wang and D. Werner, *Organometallics*, 2015, **34**, 5624–5636.
15 M. Liu, Y.-C. Chen, H. Wang, T. Shang, M.-L. Tong, R. A. Layfield, A. Mansikkamäki and F.-S. Guo, *J. Am. Chem. Soc.*, 2025, **147**, 18307–18316.
16 C. Ruspic, J. R. Moss, M. Schürmann and S. Harder, *Angew. Chem., Int. Ed.*, 2008, **47**, 2121–2126.
17 K. Kawasaki, R. Sugiyama, T. Tsuji, T. Iwasa, H. Tsunoyama, Y. Mizuhata, N. Tokitoh and A. Nakajima, *Chem. Commun.*, 2017, **53**, 6557–6560.
18 M. Xémard, S. Zimmer, M. Cordier, V. Goudy, L. Ricard, C. Clavaguéra and G. Nocton, *J. Am. Chem. Soc.*, 2018, **140**, 14433–14439.
19 T. Vitova, H. Ramanantoanina, B. Schacherl, L. Münzfeld, A. Hauser, R. S. K. Ekanayake, C. Y. Reitz, T. Prüßmann, T. S. Neill, J. Göttlicher, R. Steininger, V. A. Saveleva, M. W. Haverkort and P. W. Roesky, *J. Am. Chem. Soc.*, 2024, **146**, 20577–20583.
20 J. Rausch, C. Apostolidis, O. Walter, V. Lorenz, C. G. Hrib, L. Hilfert, M. Kühling, S. Busse and F. T. Edelmann, *New J. Chem.*, 2015, **39**, 7656–7666.
21 F. T. Edelmann, *New J. Chem.*, 2011, **35**, 517–528.
22 J. J. Le Roy, S. I. Gorelsky, I. Korobkov and M. Murugesu, *Organometallics*, 2015, **34**, 1415–1418.
23 W. J. Evans, M. A. Johnston, M. A. Greci and J. W. Ziller, *Organometallics*, 1999, **18**, 1460–1464.
24 A. Edelmann, S. Blaurock, V. Lorenz, L. Hilfert and F. T. Edelmann, *Angew. Chem., Int. Ed.*, 2007, **46**, 6732–6734.
25 A. Edelmann, V. Lorenz, C. G. Hrib, L. Hilfert, S. Blaurock and F. T. Edelmann, *Organometallics*, 2013, **32**, 1435–1444.
26 L. Münzfeld, A. Hauser, P. Hädinger, F. Weigend and P. W. Roesky, *Angew. Chem., Int. Ed.*, 2021, **60**, 24493–24499.
27 L. Münzfeld, S. Gillhuber, A. Hauser, S. Lebedkin, P. Hädinger, N. D. Knöfel, C. Zovko, M. T. Gamer, F. Weigend, M. M. Kappes and P. W. Roesky, *Nature*, 2023, **620**, 92–96.
28 W. J. Evans, J. L. Shreeve and J. W. Ziller, *Polyhedron*, 1995, **14**, 2945–2951.
29 J. Moutet, J. Schleinitz, L. La Droitte, M. Tricoire, F. Pointillart, F. Gendron, T. Simler, C. Clavaguéra, B. Le Guennic, O. Cador and G. Nocton, *Angew. Chem., Int. Ed.*, 2021, **60**, 6042–6046.
30 S. A. Kinsley, A. Streitwieser, Jr. and A. Zalkin, *Organometallics*, 1985, **4**, 52–57.
31 X. Sun and P. W. Roesky, *Inorg. Chem. Front.*, 2023, **10**, 5509–5516.
32 J. Liu, K. Singh, S. Dutta, Z. Feng, D. Koley, G. Tan and X. Wang, *Dalton Trans.*, 2021, **50**, 5552–5556.
33 Z. Dong, L. Albers and T. Müller, *Acc. Chem. Res.*, 2020, **53**, 532–543.
34 M. Saito, *Acc. Chem. Res.*, 2018, **51**, 160–169.
35 J. Wei, W.-X. Zhang and Z. Xi, *Chem. Sci.*, 2018, **9**, 560–568.
36 T. Kuwabara, J.-D. Guo, S. Nagase, T. Sasamori, N. Tokitoh and M. Saito, *J. Am. Chem. Soc.*, 2014, **136**, 13059–13064.
37 X. Sun, L. Münzfeld, D. Jin, A. Hauser and P. W. Roesky, *Chem. Commun.*, 2022, **58**, 7976–7979.
38 S. De, A. Mondal, J. Pitcairn, L. Clark, J. Tang, A. Mansikkamäki and R. A. Layfield, *Angew. Chem.*, 2025, **137**, e202502455.
39 S. De, A. Mondal, J. Tang and R. A. Layfield, *Angew. Chem., Int. Ed.*, 2025, e202516323.
40 L. Münzfeld, X. Sun, S. Schlittenhardt, C. Schoo, A. Hauser, S. Gillhuber, F. Weigend, M. Ruben and P. W. Roesky, *Chem. Sci.*, 2022, **13**, 945–954.
41 S. De, A. Mondal, S. R. Giblin and R. A. Layfield, *Angew. Chem., Int. Ed.*, 2024, **63**, e202317678.
42 S. De, A. Mondal, Z.-Y. Ruan, M.-L. Tong and R. A. Layfield, *Chem. – Eur. J.*, 2023, **29**, e202300567.
43 X. Sun, S. Schlittenhardt, T. Ruan, M. Saito, M. Ruben and P. W. Roesky, *Commun. Chem.*, 2025, **8**, 368.
44 X. Sun, A. Hinz, S. Maier, S. Gillhuber, D. Jin, M. Saito, F. Weigend, S. Schlittenhardt, E. Moreno-Pineda, W. Wernsdorfer, M. Ruben and P. W. Roesky, *Nat. Chem.*, 2026, **18**, 872–881.
45 Z. Dong, C. R. W. Reinhold, M. Schmidtmann and T. Müller, *Organometallics*, 2018, **37**, 4736–4743.
46 Y. J. Franzke, C. Holzer, J. H. Andersen, T. Begušić, F. Bruder, S. Coriani, F. Della Sala, E. Fabiano, D. A. Fedotov, S. Fürst, S. Gillhuber, R. Grotjahn, M. Kaupp, M. Kehry, M. Krstić, F. Mack, S. Majumdar, B. D. Nguyen, S. M. Parker, F. Pauly, A. Pausch, E. Perlt, G. S. Phun, A. Rajabi, D. Rappoport, B. Samal, T. Schrader, M. Sharma, E. Tapavicza, R. S. Treß, V. Voora, A. Wodyński, J. M. Yu, B. Zerulla, F. Furche, C. Hättig, M. Sierka, D. P. Tew and F. Weigend, *J. Chem. Theory Comput.*, 2023, **19**, 6859–6890.
47 TURBOMOLE V. 7.7 (University of Karlsruhe and Forschungszentrum Karlsruhe GmbH, 1989-2007, TURBOMOLE GmbH since 2007. Available from https://turbomole.org, 2021.
48 J. P. Perdew, M. Ernzerhof and K. Burke, *J. Chem. Phys.*, 1996, **105**, 9982–9985.
49 C. Adamo and V. Barone, *J. Chem. Phys.*, 1999, **110**, 6158–6170.
50 F. Weigend and R. Ahlrichs, *Phys. Chem. Chem. Phys.*, 2005, **7**, 3297–3305.
51 A. E. Reed, R. B. Weinstock and F. Weinhold, *J. Chem. Phys.*, 1985, **83**, 735–746.
52 N. Schwarz, F. Bruder, V. Bayer, E. Moreno-Pineda, S. Gillhuber, X. Sun, J. van Slageren, F. Weigend and P. W. Roesky, *Nat. Commun.*, 2025, **16**, 983.
53 J. Jusélius, D. Sundholm and J. Gauss, *J. Chem. Phys.*, 2004, **121**, 3952–3963.
54 H. Fliegl, S. Taubert, O. Lehtonen and D. Sundholm, *Phys. Chem. Chem. Phys.*, 2011, **13**, 20500–20518.
55 S. Taubert, D. Sundholm and J. Jusélius, *J. Chem. Phys.*, 2011, **134**, 054123.
56 (*a*) CCDC 2570264: Experimental Crystal Structure Determination, 2026, DOI: 10.5517/ccdc.csd.cc2s8krd; (*b*) CCDC 2570265: Experimental Crystal Structure Determination, 2026, DOI: 10.5517/ccdc.csd.cc2s8ksf; (*c*) CCDC 2570266: Experimental Crystal Structure Determination, 2026, DOI: 10.5517/ccdc.csd.cc2s8ktg; (*d*) CCDC 2570267: Experimental Crystal Structure Determination, 2026, DOI: 10.5517/ccdc.csd.cc2s8kvh; (*e*) CCDC 2570268: Experimental Crystal Structure Determination, 2026, DOI: 10.5517/ccdc.csd.cc2s8kwj; (*f*) CCDC 2570269: Experimental Crystal Structure Determination, 2026, DOI: 10.5517/ccdc.csd.cc2s8kxk; (*g*) CCDC 2570270: Experimental Crystal Structure Determination, 2026, DOI: 10.5517/ccdc.csd.cc2s8kyl; (*h*) CCDC 2570271: Experimental Crystal Structure Determination, 2026, DOI: 10.5517/ccdc.csd.cc2s8kzm; (*i*) CCDC 2570272: Experimental Crystal Structure Determination, 2026, DOI: 10.5517/ccdc.csd.cc2s8l0p; (*j*) CCDC 2570273: Experimental Crystal Structure Determination, 2026, DOI: 10.5517/ccdc.csd.cc2s8l1q; (*k*) CCDC 2570274: Experimental Crystal Structure Determination, 2026, DOI: 10.5517/ccdc.csd.cc2s8l2r.